

Crossover from ballistic to normal heat transport in the ϕ^4 lattice: If nonconservation of momentum is the reason, what is the mechanism?

Daxing Xiong,^{1,*} Danial Saadatmand,^{2,†} and Sergey V. Dmitriev^{3,4,‡}

¹*Department of Physics, Fuzhou University, Fuzhou 350108, Fujian, China*

²*Department of Physics, University of Sistan and Baluchestan, Zahedan, Iran*

³*Institute for Metals Superplasticity Problems of RAS, Khalturin St. 39, 450001 Ufa, Russia*

⁴*National Research Tomsk State University, Lenin Avenue 36, 634050 Tomsk, Russia*

Anomalous (non-Fourier's) heat transport is no longer just a theoretical issue since it has been observed experimentally in a number of low-dimensional nanomaterials, such as SiGe nanowires, carbon nanotubes, and others. To understand these anomalous behaviors, exploring the microscopic origin of normal (Fourier's) heat transport is a fascinating theoretical topic. However, this issue has not yet been fully understood even for one-dimensional (1D) model chains, in spite of a great amount of thorough studies done to date. From those studies it has been widely accepted that the conservation of momentum is a key ingredient to induce anomalous heat transport, while momentum-nonconserving systems usually support normal heat transport where Fourier's law is valid. But if the nonconservation of momentum is the reason, what is the underlying microscopic mechanism for the observed normal heat transport? Here we carefully revisit a typical 1D momentum-nonconserving ϕ^4 model and present evidence that the mobile discrete breathers or, in other words, the moving intrinsic localized modes with frequency components above the linear phonon band can be responsible for that.

I. INTRODUCTION

As one of the vivid examples for studying the microscopic origin of the macroscopic irreversibility in terms of deterministic dynamics, heat transport in one-dimensional (1D) lattice systems has attracted intensive theoretical studies for several decades [1–3]. A challenging problem here is to justify the microscopic origin of the Fourier's law, which states

$$J = -\kappa \frac{\partial T}{\partial x}, \quad (1)$$

where J is the heat current, κ is the material constant called thermal conductivity, and $\frac{\partial T}{\partial x}$ is the spatial temperature gradient. However, in a number of theoretical studies, it has been demonstrated that for general 1D lattices, κ is not just an intrinsic property of a material but depends on the chain's length L following $\kappa \sim L^\alpha$ with $0 \leq \alpha \leq 1$. The limiting case of $\alpha = 1$ corresponds to the ballistic thermal transport and for $\alpha = 0$ one has normal heat conduction obeying Fourier's law, whereas the cases of $0 < \alpha < 1$ are usually called the superdiffusive heat transport.

With the development of laser technology [4, 5] which allows to probe the thermal properties of materials at reduced size and time scales, ballistic thermal conduction ($\alpha = 1$) has been observed experimentally for Si_{0.9}Ge_{0.1} and Si_{0.4}Ge_{0.6} nanowires, carbon nanotubes, holey silicon, Al_{0.1}Ga_{0.9}N thin film, and others [6–11]. In those studies, this ballistic phonon transport has been found

for (quasi)-1D samples having length less than a threshold value, L^* (usually characterized by the phonon mean free path), such as that for SiGe nanowires $L^* \approx 8.3 \mu\text{m}$ [9], for carbon nanotubes $L^* \approx 1 \text{ mm}$ [7], and for holey silicon $L^* \approx 200 \text{ nm}$ [10]. Thus, these studies suggest that the ballistic thermal conduction in real (quasi)-1D materials can persist over macroscopic distances. In fact, it has been usually believed that in such materials heat is conducted ballistically by the low-frequency, long-wavelength phonons [6], and hence the anomalous ballistic behavior can persist even with the presence of defects, isotopic disorders, impurities, and surface adsorbates [7].

Beyond ballistic transport, the superdiffusive conduction ($0 < \alpha < 1$), can be found when the samples' length and time scales are comparable to the phonon mean free path, in particular in some nanoparticle embedded semiconductor alloys [12, 13]. Although this is just a transient process and finally the normal diffusive behavior ($\alpha = 1$) will appear as the length and time scales increase further, this superdiffusive heat transport is very peculiar and can be understood by a truncated Lévy formalism [12–15], thus suggesting a fractal Lévy heat transport physics rather than the usual Brownian motion.

To further interpret this transition from ballistic to normal behavior, a recent proposed kinetic-collective model [16] based on different phonon-phonon scattering physics might be worthwhile, from which a wide range of temperature- and size-dependent thermal conductivity can be predicted quite well [16–18]. However, obviously such a theoretical model does not involve the effects of other nonlinear excitations, such as solitons [19] and discrete breathers (DBs) [20–23].

In addition to the experimental investigations, there are also a number of molecular dynamics studies on quasi-1D and 2D nanomaterials [24–27]. Such studies showed that the rough edges of long graphene nanorib-

*Electronic address: phyxiongdx@fzu.edu.cn

†Electronic address: saadatmand.d@gmail.com

‡Electronic address: dmitriev.sergey.v@gmail.com

bons suppress thermal conductivity by two orders of magnitude [24]. Isolated carbon nanotube demonstrates anomalous heat transport due to the long-wavelength acoustic phonons, while nanotube interacting with a flat substrate displays normal thermal conductivity due to both the appearance of a gap in the acoustic phonon spectrum and the absorption of long-wavelength acoustic phonons by the substrate [25]. Isotopic doping decreases thermal conductivity of silicene nanosheets [26].

Coming back to 1D model chains, up to now, many ingredients related to anomalous thermal conduction have been carefully considered, among them are chaos [28–33], conservation of momentum [34–37], asymmetric interactions [38–42], linearity [33, 43–46], integrability [47], pressure [48, 49], surface scattering effect [50] etc. Particularly, the viewpoint that a system with (without) a momentum conservation property should disobey (obey) Fourier’s law has been widely accepted, although there are still some contradictory results on this issue [51–59]. A suggested picture to support this viewpoint is that the on-site potentials which destroy the conservation of momentum can induce a strong scattering mechanism for phonons, eventually resulting in the diffusive Fourier’s heat transport. In some literature [60, 61], such scattering mechanism is usually attributed to DBs. Nevertheless, at present, our understanding of the physical picture of this scattering process is still lacking.

In this work we therefore revisit a typical momentum-nonconserving system, i.e., the ϕ^4 model with a single-well on-site potential. Keeping in mind that only the nonlinear on-site potential can result in normal heat transport [33], we shall carefully examine both the system’s heat transport and DBs properties under different strengths of the nonlinearity, trying to establish a connection between them. Our aim is to present a possible mechanism for demonstration why a system with non-conserved momentum can generally lead to normal heat transport.

The rest of this article is organized as follows: In Sec. II we first introduce the reference model, demonstrate its linear phonon dispersion, and discuss what kind of DBs are likely to exist for the given type of nonlinearity. Sec. III then describes our numerical approaches used in the heat transport study. In Sec. IV, we provide our main results, from which we will see a close relationship between heat transport and DBs properties, with the change of the strength of the nonlinearity. Sec. V presents a discussion and finally Sec. VI draws our conclusions.

II. MODEL

The Hamiltonian of 1D ϕ^4 lattice is given by

$$H = \sum_{k=1}^L \frac{p_k^2}{2} + V(\phi_{k+1} - \phi_k) + U(\phi_k). \quad (2)$$

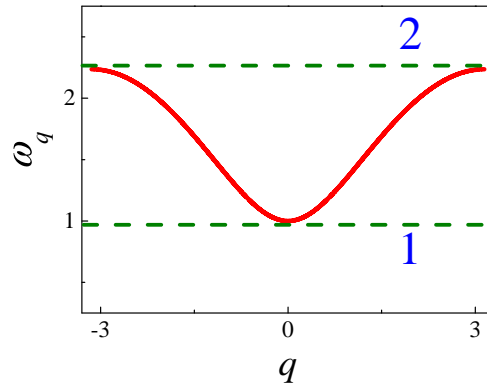


FIG. 1: The phonon dispersion relation for the ϕ^4 lattice, where the lines 1 and 2 indicate the lower and upper edges of the linear phonon band. Note that for the considered hard-type anharmonicity, only DBs with frequencies above line 2 can exist.

Here L particles are considered; all of them have unit mass; p_k is the momentum of the k th particle; ϕ_k is its displacement from equilibrium position; $V = \frac{\xi^2}{2}$ and $U = \frac{\xi^2}{2} + \beta \frac{\xi^4}{4}$ denote the harmonic interparticle interaction and the nonlinear on-site potential, respectively. Parameter β ($\beta > 0$) controls the strength of the nonlinearity in U , variation of which will help us to explore the detailed relationship between the heat transport and the DBs properties. We note that for $\beta > 0$ the on-site potential focused here is single-well and of hard-type anharmonicity.

From Eq. (2), the following equations of motion can be derived

$$\frac{d^2 \phi_k}{dt^2} = (\phi_{k-1} - 2\phi_k + \phi_{k+1}) - \phi_k - \beta \phi_k^3. \quad (3)$$

Then, under harmonic approximation ($\beta = 0$), the system’s phonon dispersion relation can be easily obtained:

$$\omega_q = \sqrt{4 \sin^2 \left(\frac{q}{2} \right) + 1}, \quad (4)$$

where q is the wave number and ω_q is the corresponding phonon frequency. Such phonon dispersion relation is shown in Fig. 1. As can be seen, unlike the linear phonon dispersion of a momentum-conserving system without including the on-site potential, the lowest wavelength phonon frequency in our case is now no longer at the zero value, instead, its frequency is shifted to the value of $\omega_q^{\min} = 1$. On the other hand, the shortest wavelength phonon frequency is equal to $\omega_q^{\max} = \sqrt{5} \approx 2.236$. Accordingly, it is easy to find that the phonon’s group velocity v_g , defined as $v_g = \frac{d\omega_q}{dq}$, vanishes for $q \rightarrow 0$ and $q \rightarrow \pm\pi$, which is a necessary condition for the excitation of DBs when including the nonlinearity.

DBs frequency must lie outside the phonon spectrum. For the hard-type nonlinearity considered ($\beta > 0$), only DBs with frequencies lying in the range denoted by 2 in Fig. 1, i.e., above the linear phonon band, are possible [20–23]. It can also be expected that, the nonlinearity

together with the phonon dispersion as shown in Fig. 1 induced by the on-site potential will make such kind of DBs properties very peculiar, different from those in the usually considered momentum-conserving systems. So, in view of these general understandings, in what follows we will examine the DBs properties at given strength of the nonlinearity, aiming to understand their relation to thermal transport.

III. METHOD

To characterize the system's thermal transport property, one can employ the equilibrium fluctuation-correlation method [62–64] to derive the spatiotemporal correlation function of heat fluctuations [65, 66]:

$$\rho_Q(m, t) = \frac{\langle \Delta Q_j(t) \Delta Q_i(0) \rangle}{\langle \Delta Q_i(0) \Delta Q_i(0) \rangle}. \quad (5)$$

Here $m = j - i$; $\langle \cdot \rangle$ represents the spatiotemporal average. $Q_i(t)$ is the heat density within a finite volume (bin i) at time t , whose expression [65, 66]

$$Q_i(t) \equiv E_i(t) - \frac{(\langle E \rangle + \langle F \rangle) M_i(t)}{\langle M \rangle} \quad (6)$$

is obtained from basic thermodynamics in the textbooks [65, 66]. To compute $Q_i(t)$, in practice one can first divide the 1D lattice into several equivalent bins. In each bin, we then calculate the number of particles M_i , the energy E_i and the pressure F_i within the bin. Finally, the heat in the i th bin can be derived from (6) and its fluctuation then is $\Delta Q_i(t) = Q_i(t) - \langle Q_i \rangle$. We note that since the system is 1D, the pressure is equal to the force and can be calculated from the gradient of the potential.

This simulation approach for deriving $\rho_Q(m, t)$ has been widely used in many publications [58, 59, 62–64, 67, 68]. In particular, from the perspective of random walks theory [62–64, 67], $\rho_Q(m, t)$ (normalized) can be viewed as the heat spreading density, which together with a space-time scaling analysis has been suggested being able to provide very detailed information for characterizing the corresponding thermal transport behavior [69]. In the hydrodynamics theory, $\rho_Q(m, t)$ is believed to correspond to the heat mode's correlation [67, 70].

To simulate $\rho_Q(m, t)$, we consider a chain with $L = 4001$ particles, which allows an initial heat fluctuation located at the center to spread out a lag time at least up to $t = 1500$. This is because the introduction of the on-site potential reduces the group velocity of phonons as compared to the momentum-conserving harmonic chain (its phonon group velocity is unity). We set both the equilibrium distance between the particles as well as the lattice constant to unity. This means that the number of particles L is equal to the system size. So, for a system with symmetric (even) type interactions, it can be easily inferred that the average pressure $\langle F \rangle$ is always zero. We apply periodic boundary conditions and fix the number

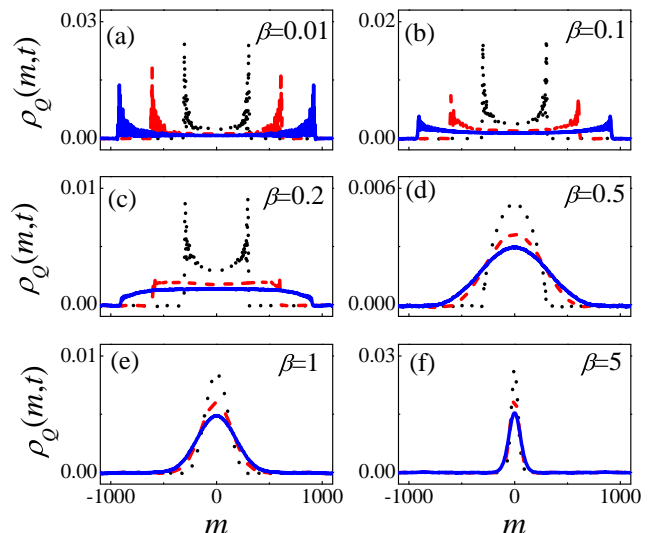


FIG. 2: $\rho_Q(m, t)$ calculated for several β values at three typical long times $t = 500$ (dotted); $t = 1000$ (dashed), and $t = 1500$ (solid).

of bins to be $(L - 1)/2$. We use the stochastic Langevin heat baths [1, 2] to thermalize the system and to prepare a canonical equilibrium state with a fixed temperature $T = 0.5$. The nonlinear parameter β is varied over a wide range from $\beta = 0.01$ to $\beta = 5$. Under this setup, we employ the Runge-Kutta algorithm of seventh to eighth order with a time step of $h = 0.05$ to evolve the system. Each canonical equilibrium system is prepared by evolving the system for a long enough time ($> 10^7$ time units) from properly assigned initial random states. Finally, we use ensembles of about 8×10^9 data points to compute the correlation function.

IV. RESULTS

A. Heat transport

We first present several β -dependent profiles of $\rho_Q(m, t)$ for three long times in Fig. 2. As can be seen, indeed only including a strong enough nonlinearity can lead to the perfect Gaussian profile of $\rho_Q(m, t)$ [see Fig. 2(f)], which is an evidence of normal thermal transport obeying Fourier's law. This is consistent with the argument that the linear optical chain, even with nonconserved momentum, cannot exhibit normal heat transport [33]. One can also find that for relatively small nonlinearity, $\rho_Q(m, t)$ shows a U-shape with some oscillations [see Fig. 2(a)]. This is a typical signature of ballistic heat transport and can be predicted by a recent theory of “phonon random walks” [71]. In addition, in the intermediate range of the nonlinearity, there is a transition (crossover) from ballistic to normal transport [see Fig. 2(b)-(e)], i.e., with the increase of β , at first the front peaks of $\rho_Q(m, t)$ are quickly damped, then after this damping process has been almost finished, the central part of $\rho_Q(m, t)$ starts

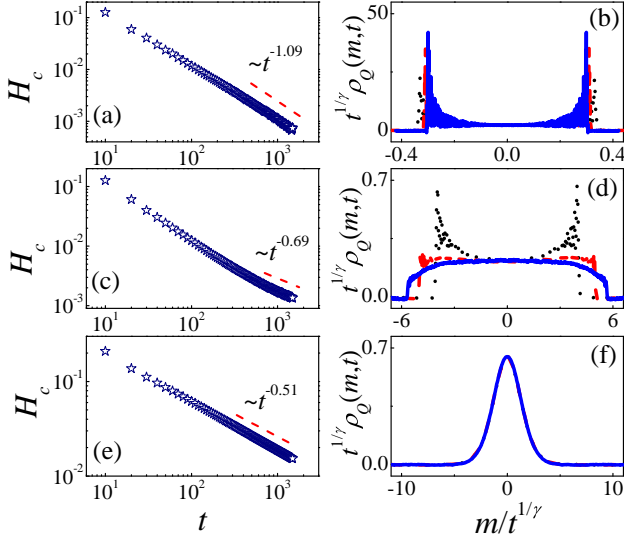


FIG. 3: Left: (a), (c) and (e), the height H_c of the central peaks of $\rho_Q(m, t)$ vs t for extracting the scaling exponent γ ; Right: (b), (d) and (f), the rescaled $\rho_Q(m, t)$ using formula (7), where (a) and (b) for $\beta = 0.01$; (c) and (d) for $\beta = 0.2$; (e) and (f) for $\beta = 5$, respectively. In (b), (d) and (f), three typical long times of $t = 500$ (dotted); $t = 1000$ (dashed), and $t = 1500$ (solid) are compared.

to be humped and seems more and more concentrated.

We are particularly interested in this transition process in the intermediate range of β . So, we perform a space-time scaling analysis [63, 64]

$$\rho_Q(m, t) \simeq \frac{1}{t^{1/\gamma}} \rho_Q\left(\frac{m}{t^{1/\gamma}}, t\right) \quad (7)$$

of the central part of $\rho_Q(m, t)$ for different β values. Three typical results of the rescaled $\rho_Q(m, t)$ are shown in Fig. 3(b)(d)(f). According to the random walk theory [63, 64], the scaling exponent γ can be extracted from the time scaling behavior of the height H_c of the central peaks of $\rho_Q(m, t)$ [see Fig. 3(a)(c)(e)] and related to the system size scaling exponent α of heat conductivity by $\alpha = 2 - \gamma$ [63, 64]. Hence, $\gamma = 1$ and $\gamma = 2$ correspond to the ballistic and normal transport, respectively [63, 64]. So, given these scaling exponents, Fig. 3(b) [(f)] indicates the heat transport close to ballistic (normal); Fig. 3(d) suggests a crossover process.

To readily capture this crossover process, we also plot the result of γ versus β in Fig. 4. This helps us to more precisely infer the transition point. As can be seen, Fig. 4 suggests that the transition point is in between $\beta = 0.1$ and $\beta = 0.4$. As to this point, we note that $\beta = 0.2$ is just a central point among them, which is consistent with the result in Fig. 2(c), where the front peaks of $\rho_Q(m, t)$ are nearly completely damped for a relatively long time. In the very long time and with very long size simulation, one may thus expect that $\beta_c = 0.2$ is probably a transition point for the system's heat transport crossover from ballistic to normal at the focused temperature $T = 0.5$.

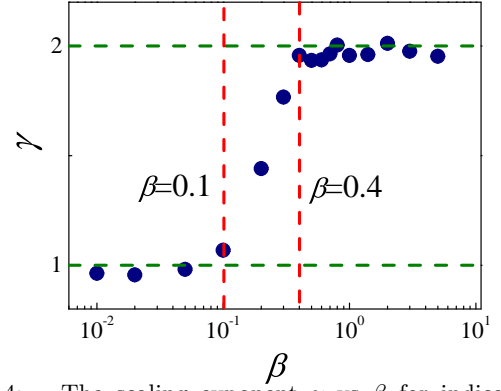


FIG. 4: The scaling exponent γ vs β for indicating the crossover process from ballistic to normal heat transport, where horizontal lines, from bottom to top, denote $\gamma = 1$ and $\gamma = 2$; the vertical lines, from left to right, represent $\beta = 0.1$ and $\beta = 0.4$, respectively.

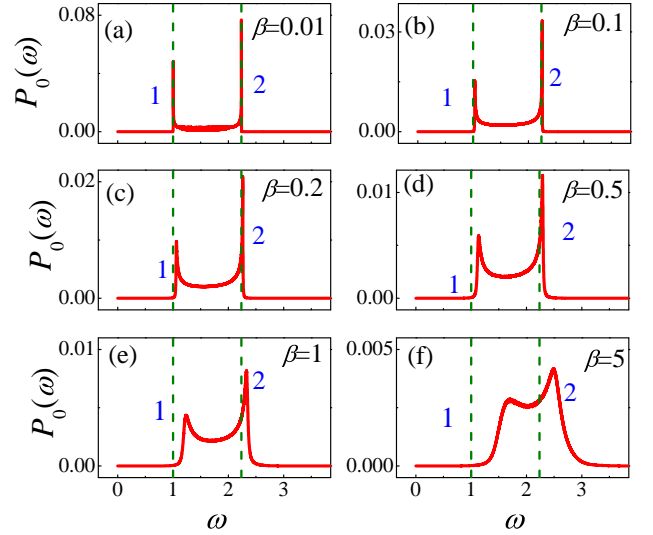


FIG. 5: The power spectrum $P_0(\omega)$ of the equilibrium states at $T = 0.5$ for the chains with different strengths of the non-linearity: (a) $\beta = 0.01$, (b) $\beta = 0.1$, (c) $\beta = 0.2$, (d) $\beta = 0.5$, (e) $\beta = 1$, and (f) $\beta = 5$. The lower and the upper boundaries of the linear phonon band are shown by the vertical dashed lines and indicated as 1 and 2, respectively.

B. DBs properties

Next, we attempt to relate the observed β -dependent heat transport behavior to the β dependence of DBs properties. For this aim, we will study DBs properties at both finite and zero temperatures.

1. Evidence for DBs in thermalized chains for $\beta \geq 0.5$

We first thermalize the focused systems of size $L = 200$ (for facilitating the calculation) to the desired temperature $T = 0.5$ with the Langevin heat baths [1, 2]. Then, the thermostats are turned off and the power spectrum $P_0(\omega)$ of these thermal oscillations are calculated. In Fig. 5 we present the result of $P_0(\omega)$ versus ω for sev-

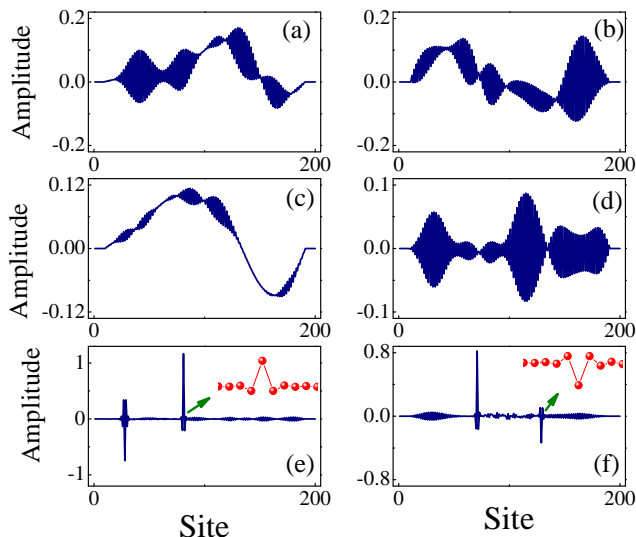


FIG. 6: Several typical snapshots of the residual thermal fluctuations after a long time's absorption for three β values, where (a)-(b) for $\beta = 0.01$, (c)-(d) for $\beta = 0.2$, and (e)-(f) for $\beta = 5$. The insets in (e) and (f) are used for indicating the Sievers-Takeno DB modes.

eral β values. As can be seen, for $\beta \geq 0.5$ a notable blueshift of $P_0(\omega)$ towards the direction of higher frequencies is observed [see Fig. 5(d)]. This is the signature of appearance of the hard-type anharmonicity DBs with frequencies above the linear phonon band, i.e., in the region marked by 2 in Fig. 5. The appearance of the blueshift of $P_0(\omega)$ for $\beta \geq 0.5$ coincides with the result of Fig. 4 where the transition from ballistic to normal heat transport takes place at about $\beta = 0.1$ -0.4. Depletion of $P_0(\omega)$ in the long-wavelength region at large β [see Fig. 5(d)-(f)] can also be explained by the appearance of DBs. Indeed, DBs act as the pins cutting the chain into the parts and reducing the room available for the long-wavelength phonons.

2. Application of absorbing boundary conditions

There exists a numerical method which directly demonstrates the existence of DBs in thermalized lattices [60, 61]. To use this approach, again a system of size $L = 200$ is thermalized to $T = 0.5$. Then, the thermostat is turned off, but now the absorbing boundary conditions are imposed for a long enough time. With such strategy, all the mobile excitations will be absorbed by the boundaries, while the immobile DBs can show up if they exist. Finally, one then can calculate the power spectrum $P(\omega)$ of these residual oscillations to identify the corresponding immobile DBs frequencies.

In Fig. 6 we show several snapshots of the residual thermal fluctuations after a long time's absorption for three typical β values. For each β , two typical results from two different initial equilibrium states of the same focused temperature are compared. Interestingly, one can see a

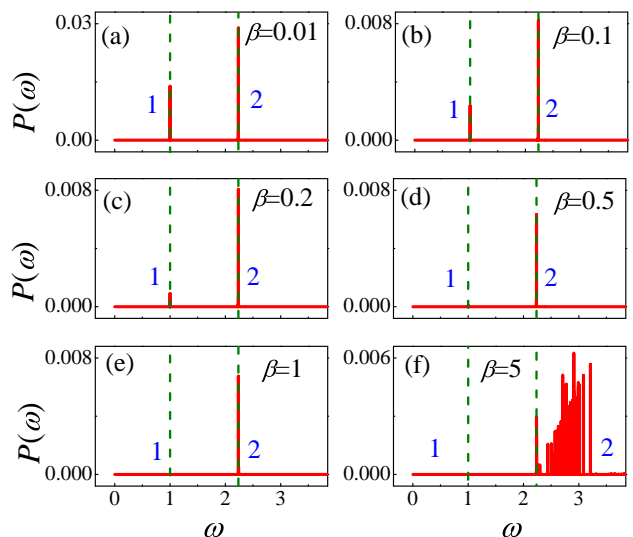


FIG. 7: The power spectrum $P(\omega)$ of the residual thermal fluctuations after a long time's absorption: (a) $\beta = 0.01$, (b) $\beta = 0.1$, (c) $\beta = 0.2$, (d) $\beta = 0.5$, (e) $\beta = 1$, and (f) $\beta = 5$, where the vertical dashed lines 1 and 2 shown the lower and upper edges of the linear phonon band, respectively.

variation of such snapshots with β as well, i.e., for relatively large nonlinearity, we always have the chance to observe several highly localized modes [see Fig. 6(e)-(f)]. These modes can be characterized as immobile, stationary DBs centered on a particle, i.e., the so-called Sievers-Takeno (ST) modes [72]. For relatively small nonlinearity, the residual thermal fluctuations are the mixture of phonons with q close to zero and to the zone boundary ($q = \pm\pi$) [see Fig. 6(a)-(d)]. This is expected since such phonons have vanishing group velocity and they remain in the system after long exposure to the absorbing boundary conditions.

We then study the power spectrum $P(\omega)$ of these residual thermal fluctuations in order to get the information of their frequencies. The result of $P(\omega)$ versus ω is shown in Fig. 7. Here, similar to Fig. 5, different values of β are indicated in each panel. From Fig. 7, first at a relatively small β ($\beta = 0.01$), both the peaks corresponding to the phonons with frequencies close to $q = 0$ (denoted by type 1) and to the zone boundary (type 2) can be clearly identified [see Fig. 7(a)]. This may explain why the U-shape can be seen in Fig. 2(a). Then, with the slight increase of β ($\beta = 0.1$ and $\beta = 0.2$), the type 1 frequency component becomes weaker and weaker but there is almost no change for the type 2 frequency component [see Fig. 7(b)-(c)], which seems related to the quick damping of the front peaks of $\rho_Q(m, t)$ shown in Fig. 2(b)-(c). In Fig. 7(d) and (e), the peak corresponding to phonons with longest wavelengths becomes very weak but the peak for the shortest wavelengths remains, which might indicate the broader Gaussian peak of $\rho_Q(m, t)$ as shown in Fig. 2(d) and (e). Finally, for the case of strong nonlinearity ($\beta = 5$) [see Fig. 7(f)], one can clearly see the excitations with frequencies above the linear phonon

band indicating the presence of immobile DBs in the system in line with Fig. 6(e)-(f). These immobile DBs seem to have the effects to make the Gaussian peak $\rho_Q(m, t)$ narrower [see Fig. 2(f)]. All of these evidences clearly show the strong correlation between β -dependent DBs properties and heat transport, suggesting that in this particular system with nonconserved momentum, exploring DBs properties could be very helpful for understanding heat transport. That may be also why, previously, researchers often used the role of DBs as a major phonons scattering mechanism to understand the diffusive heat conduction in the momentum-nonconserving systems [60, 61].

Given the strong correlation between the results of Figs. 2 and 7, now it is reasonable to assume that DBs are responsible for the transition to the normal heat transport at large β , since in Fig. 7 the role of phonon-phonon interaction has almost been ruled out, in view of applying the absorbing boundary conditions. However, the absence of DBs frequencies in Fig. 7(d) and (e) should be considered puzzling, because at $\beta = 0.5$ and $\beta = 1$, according to Fig. 4, we already have normal heat transport obeying Fourier's law. Thus, in the following we need to find an explanation why DBs cannot be seen in the chain after long action of absorbing boundary conditions for $\beta = 1$ and why they are still presented for $\beta = 5$. Our viewpoint about this is that it may be related to the DBs mobility, i.e., at the focused temperature, when $\beta = 1$, the mobile DBs are excited, whereas for $\beta = 5$, the immobile DBs dominate. They have different properties, i.e., the mobile DBs can be scattering with the lowest-frequency phonons, while after this scattering has been almost finished, the immobile DBs emerge and their main role is to localize energy and heat. So, when the absorbing boundary conditions are imposed, eventually only the immobile DBs can be identified. As we will show this seems to be verified in the following.

3. DBs at zero temperature: Standing DBs

With the above puzzle in mind, i.e., the absence of DB frequencies in Fig. 7(d)(e), we next explore DBs properties at zero temperature (for facilitating the analysis). As mentioned, our main goal is to explain why standing DBs remain in the chain after applying absorbing boundary conditions in the case of $\beta = 5$, while they cannot be seen for $\beta = 1$, cf., (e) and (f) in Fig. 7.

We first focus on the properties of standing DBs and in the following we will try to boost them. An efficient way to excite such type of standing DBs is the use of the following initial conditions

$$\phi_k(0) = \frac{(-1)^k A_{\text{DB}}}{\cosh[\theta(k - x_0)]}, \quad \frac{d\phi_k(0)}{dt} = 0. \quad (8)$$

Here, A_{DB} and θ are the DB's amplitude and inverse width, respectively. DB's initial position is located at x_0 and for $x_0 = (L-1)/2$ [$x_0 = (L+1)/2$] the DB is centered on a particle (at the center of a bond). We always took

$x_0 = (L-1)/2$ to obtain the ST mode observed in our simulations. For the chosen A_{DB} , we find θ by using the try and error method [73] minimising the oscillations of the DB's amplitude in simulations. After θ has been found, we then calculate DB's frequency, ω_{DB} , and its total (kinetic plus potential) energy, E_{DB} . These results are presented in Table I for a set of DB's amplitudes for the focused two values of $\beta = 1$ and $\beta = 5$.

From Table I it can be seen that, with the increase of DB's amplitude, the degree of its spatial localization, characterized by θ , increases. The same is true for both the DB's frequency and energy. In addition, DBs of the same amplitude in the chain with higher strength of the nonlinearity have higher spatial localization and higher frequency. However, this is not the case for the DB's energy. Within the studied range of amplitudes, the energy of DBs with same amplitude in the chain with weaker nonlinearity is larger, which shows a big difference between the cases of $\beta = 1$ and $\beta = 5$. This is consistent with the results of Fig. 5(e) and (f), where the spectrum energies in the case of $\beta = 1$ are obviously larger than the counterparts of $\beta = 5$. Regardless of this difference, in short, all of the data indicate the concentration of energies played by DBs as shown in Fig. 2(f) for the relatively large strengths of the nonlinearity.

4. DBs at zero temperature: Moving DBs

Moving DBs were excited with the use of the following physically motivated ansatz [73]:

$$\phi_k(t) = \frac{(-1)^k A_{\text{DB}} \cos[\omega_{\text{DB}} t + \delta(k - x_0)]}{\cosh[\theta(k - x_0)]}. \quad (9)$$

Here, δ is a free parameter which defines the oscillation phase difference for neighboring particles and also characterizes DB's velocity, v_{DB} , in case when it is mobile. For example, for $\delta = 0$, DB's velocity is zero.

$\beta = 1$			
A_{DB}	θ	ω_{DB}	E_{DB}
0.25	0.154	2.240	2.028
0.5	0.309	2.257	4.091
0.75	0.474	2.282	6.069
1.0	0.639	2.319	8.147
1.25	0.871	2.354	9.487
1.5	1.135	2.410	10.744

$\beta = 5$			
A_{DB}	θ	ω_{DB}	E_{DB}
0.25	0.349	2.262	0.909
0.5	0.748	2.332	1.751
0.75	1.360	2.451	2.318
1.0	1.960	2.687	3.570
1.25	2.441	3.009	6.091
1.5	2.814	3.380	10.344

TABLE I: The standing DB's relevant parameters.

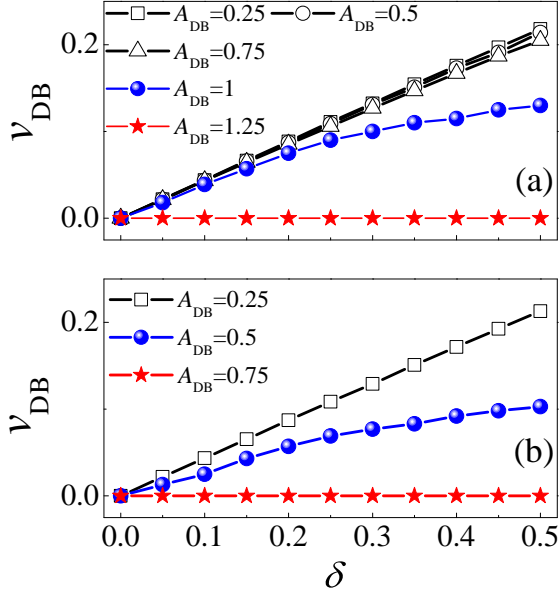


FIG. 8: Velocity v_{DB} of DBs excited with the help of the ansatz Eq. (9) as a function of δ : (a) $\beta = 1$ and (b) $\beta = 5$. DB's amplitude is indicated in the legends. Other DB's parameters are taken from Table I.

We use Eq. (9) with different values of δ for setting the initial conditions taking other DB's parameters from Table I. Velocity of the resulting DB is measured and presented as a function of δ in Fig. 8(a) and (b) for the chains with $\beta = 1$ and $\beta = 5$, respectively. Different lines show the results for different DB's amplitudes A_{DB} , as indicated in the legends. It can be seen that DBs with relatively small amplitudes have velocities nearly proportional to δ within the range of $|\delta| \leq 0.5$ considered. For $\beta = 1$, this is true for $A_{DB} \leq 0.75$, while for $\beta = 5$ it is observed for $A_{DB} \leq 0.25$. Such DBs are highly mobile. We have checked that they move through entire computational cell of 3000 sites with nearly constant velocity and practically radiating no energy. However, for the cases of, e.g., $A_{DB} = 1$ ($\beta = 1$) and $A_{DB} = 0.5$ ($\beta = 5$), DB's velocity saturates with the increase of δ , it radiates small-amplitude waves, and its velocity gradually decreases. For this reason, we can only measure the DB's velocity up to $t = 400$. Finally, DBs with even higher amplitudes are trapped by the lattice and no longer move for any value of δ . This is observed for $A_{DB} \geq 1.25$ ($\beta = 1$) and $A_{DB} \geq 0.75$ ($\beta = 5$).

Combining the results presented in Fig. 8 and the DB's parameters shown in Table I, now one may recognize that the immobility of DBs takes place for about $\theta \geq 0.7$. Indeed, Table I indicates that, for $A_{DB} = 1$ ($\beta = 1$), one has $\theta = 0.639$; and for $A_{DB} = 0.5$ ($\beta = 5$), $\theta = 0.748$. Both cases are close to the transition of DBs from mobile to immobile as suggested by Fig. 8.

It is also very interesting to note that at the transition point of $\theta \simeq 0.7$, the DB's energy for $\beta = 1$ ($E_{DB} = 8.147$) is much higher than that in the case of $\beta = 5$ ($E_{DB} = 1.751$). This may correspond to the fact that

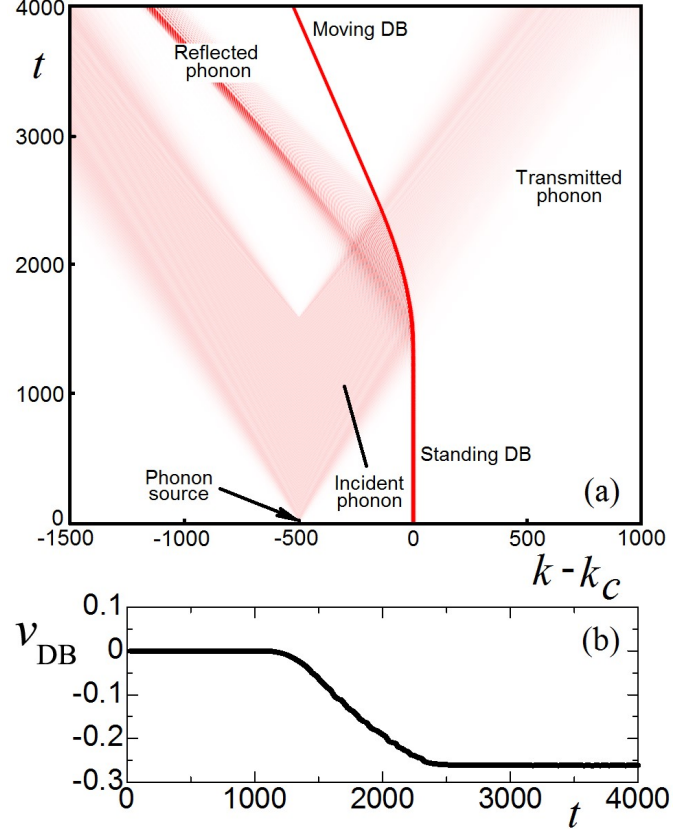


FIG. 9: (a) Counter plot showing the evolution of total (kinetic plus potential) energies of particles with t in the chain with $\beta = 1$. Initially ($t = 0$), in the center k_c , a standing DB is excited by using ansatz (9) with $A_{DB} = 0.5$, $\delta = 0$, $\omega_{DB} = 2.257$ and $\theta = 0.309$, and an ac driving phonon source at $k^* = k_c - 500$ is operated until $t = 1500$. One can see that the DB is accelerated towards the phonon source during the scattering with the phonon wave packet. (b) Time evolution of DB's velocity during this process.

the probability of excitation of immobile DBs for $\beta = 1$ is relatively small compared to the case of $\beta = 5$, consistent with the results shown in Fig. 7(d)-(f).

5. Acceleration of DBs by phonons

Now we understand that there are two different types of DBs existing in the system characterized by their different mobility induced by different β values together with the different A_{DB} . With this understanding, we next demonstrate that the mobile DBs can be scattered by the small-amplitude phonons. To see this, we first excite a DB in the center [$k_c = (L - 1)/2$] of the chain. As an example, we choose the case of $\beta = 1$ and set $A_{DB} = 0.5$ and $\delta = 0$, so $\theta = 0.309$ according to Table I. Thus, a mobile DB with zero initial velocity according to Fig. 8 is excited. At the same time, on the left-hand side of the DB, a particle with the index number k^* is forced

to move according to the following ac driving:

$$\phi_{k^*}(t) = A_p \sin(\omega_p t), \quad (10)$$

where A_p and ω_p are the driving amplitude and frequency, respectively. We use a relatively small A_p and set ω_p within the phonon band, so that a phonon-like wave packet with the given frequency is excited and interacts with the DB. In order to provide the details of such scattering process, we then record each particle's energy for a long time up to $t = 4000$. A typical result with the parameters $A_p = 0.075$, $\omega_p = 1.1$ and $k^* = k_c - 500$ is shown in Fig. 9(a). Under this setup, we perform the ac driving for a time lag up to $t = 1500$ and then it is stopped.

From Fig. 9(a), one can see that the incident phonon wave packet is partially reflected and partially transmits, which is reasonable. While for the DB, the result is very interesting. Due to the scattering by the phonon wave packet, the standing mobile DB is accelerated towards the phonon source. This indicates that the phonon-DB interaction can cause the mobile DB from standing to moving, and in turn provides a scattering mechanism for phonons. For more details, we also detect the time evolution of the DB's velocity, which is shown in Fig. 9(b). This result tells us that, a standing DB after interaction with the phonon wave packet moves with a constant nonzero velocity.

6. Summary of DBs properties in relation to heat transport

Now we summarize our main results on DB properties and try to relate them to heat transport. In the focused ϕ^4 model with hard-type anharmonicity ($\beta > 0$), only DBs with frequencies above the linear phonon band can exist. While including on-site potential makes these DBs properties quite peculiar, which seem distinct from those shown in the momentum-conserving systems. Our numerical analysis suggests that, (i) DBs with high degree of spatial localization ($\theta \geq 0.7$) are immobile, while less localized DBs ($\theta \leq 0.7$) are mobile. So, $\theta \approx 0.7$ is a threshold value at which DBs change from mobile to immobile. This is indeed true for the two typical cases we considered, i.e., $A_{DB} \geq 1.0$ for $\beta = 1$ and $A_{DB} \geq 0.5$ for $\beta = 5$. (ii) At the transition point of $\theta \approx 0.7$, the single DB's energy E_{DB} in the chain with $\beta = 1$ is almost five times larger than that of $\beta = 5$. Then, according to the Arrhenius law [74], the probability of DB's excitation by thermal fluctuations at a finite temperature T is proportional to $e^{-E_{DB}/(k_B T)}$, where k_B is the Boltzmann constant. This explains why for $\beta = 1$ the probability of excitation of immobile DBs is orders of magnitude smaller than in the case $\beta = 5$. So, for $\beta = 1$ DBs are mainly mobile and it is reasonable to see that they disappear after application of the absorbing boundary conditions for a long time, as evidenced in Fig. 7(e); whereas in the case of $\beta = 5$ we have a large chance to excite the immobile DBs, so they show up in Fig. 6(e)-(f)

and Fig. 7(f) after exposure to the absorbing boundary conditions for a long time. (iii) DBs can be scattered with phonons. In particular, the mobile DBs can be accelerated by the phonons as exemplified by Fig. 9. This in turn causes a scattering mechanism for phonons. So, when this scattering becomes dominant, the normal heat transport can be observed. This is indeed the case for $0.4 \leq \beta \leq 1$ as shown in Fig. 2(d) and (e). For even higher strength of the nonlinearity ($\beta = 5$ for example), the immobile DBs are readily excited and normal heat transport is now characterized by a narrower Gaussian peak, as shown in Fig. 2(f). This may suggest that the immobile DBs can localize the energy and heat.

V. DISCUSSION

Finally, we discuss why the above pictures are related to the nonconservation of momentum and what happens in the range of $\beta \leq 0.4$. For this aim we employ the momentum correlation function $\rho_p(m, t)$ to detect the relevant information. Similarly to $\rho_Q(m, t)$, $\rho_p(m, t)$ is defined by

$$\rho_p(m, t) = \frac{\langle \Delta p_j(t) \Delta p_i(0) \rangle}{\langle \Delta p_i(0) \Delta p_i(0) \rangle}. \quad (11)$$

Here $\Delta p_i(t) \equiv p_i(t) - \langle p_i \rangle$ denotes the momentum fluctuation at a bin i and time t . Simulation of this correlation function is also similar to that of $\rho_Q(m, t)$.

$\rho_p(m, t)$ has been verified to be very useful in understanding anomalous thermal transport. For example, from the perspective of hydrodynamics theory [67, 70], $\rho_p(m, t)$ has been conjectured to represent the sound modes' correlation. A diffusive behavior of $\rho_p(m, t)$ has been observed in the couple rotator systems and related to the observed normal heat transport [75]. Such non-ballistic diffusive momentum spread appears to be the origin of the recovery of Fourier's law in a special system with a double-well interparticle potential [58, 59]. A more recent work based on an effective linear stochastic structure theory [76] has indicated that the scaling behavior of $\rho_p(m, t)$ can enable us to explore the sound damping information, and thus is related to anomalous heat transport. However, all of the above results are the understanding for momentum-conserving systems, here, however, we will use $\rho_p(m, t)$ to understand the origin of normal heat transport in the momentum-nonconserving systems.

Figure 10 presents the result of $\rho_p(m, t)$ for several small β values. It is easy to find that above $\beta = 0.2$, all the correlation information of $\rho_p(m, t)$ disappear. This is so because, in this range the mobile DBs become dominated. Then, the phonons with low frequencies, i.e., the sound modes, can be completely damped due to the scattering with DBs. This is another type of signature of normal heat transport in momentum-nonconserving systems induced by the on-site potentials, different from the

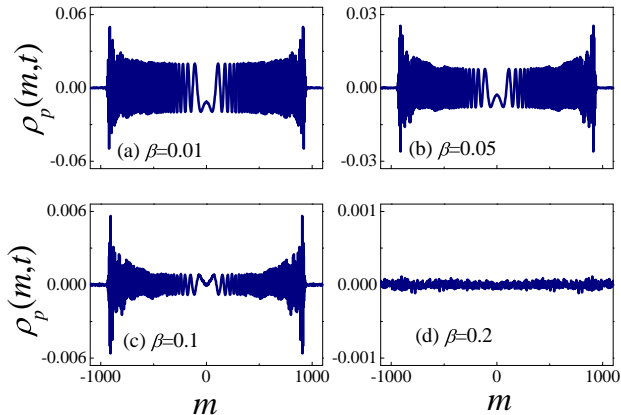


FIG. 10: The momentum correlation function $\rho_p(m, t)$ for several small β values for a long time $t = 1500$: (a) $\beta = 0.01$, (b) $\beta = 0.05$, (c) $\beta = 0.1$, and (d) $\beta = 0.2$.

diffusive behavior of $\rho_p(m, t)$ shown in some momentum-conserving systems [58, 59, 75]. In the context of hydrodynamics, it means a complete damping of the sound modes' correlation, similarly to the results of [58, 59, 75] but obviously here it is in a distinctive way.

Now, inspired by this macroscopic evidence of $\rho_p(m, t)$, we may conjecture that, with slight nonlinearity ($0.01 \leq \beta \leq 0.4$), there are also mobile DBs excited in the system. While these mobile DBs are not dominated, so, the scattering of phonons are not strong enough to cause normal heat transport. Therefore, a gradual damping of the momentum correlation information as shown in Fig. 10 can be observed. Finally, as to the full underlying picture in the whole ranges of $0.01 \leq \beta \leq 5$, we would like to suggest such an understanding: To induce normal heat transport in the momentum-nonconserving ϕ^4 system, one should resort to the nonlinearity. This nonlinearity together with the on-site potentials can cause a phonons scattering mechanism induced by the mobile DBs with frequency components slightly above the linear phonons band. For the very large nonlinearity, after the scattering process has been almost completed, another type of immobile DBs with frequency components greatly upper the linear phonon band now becomes dominated. This kind of immobile DBs can localize the energy and heat [77], which may make the system like an insulator with a very low thermal conductivity. So, a narrow Gaussian heat transport density can be observed in Fig. 2(f).

VI. CONCLUSIONS

In summary, we have succeeded in understanding the transition process to normal heat transport in the momentum-nonconserving ϕ^4 system when the strength of the hard-type nonlinearity β is increased. To do this, we have examined both the macroscopic heat transport property and the microscopic details of DBs dynamics for different β values. In general, as β increases, we have

found that, the heat transport can undergo a crossover from ballistic to normal, with some rich details, i.e., first, the ballistic moving peaks of the heat perturbations correlation are damped, and then its central part becomes more and more concentrated. Interestingly, such rich details seem to be strongly related to the microscopic DBs properties, i.e., the nonlinearity together with the on-site potential makes the system to excite both mobile and immobile DBs, respectively, at the relatively weak and strong nonlinearity. These DBs have different effects on the heat transport property. On one hand, the mobile DBs induce a scattering mechanism for phonons which results in the damping of the sound modes' correlation. Eventually, when this effect of scattering becomes dominated, a normal thermal transport obeying the Fourier's law characterized by a Gaussian-type heat transport density can be seen. On the other hand, for the relatively large nonlinearity, the main excitations are instead the immobile DBs. This kind of DBs has the effects of localizing energy and heat, making the chain like an insulator, and finally reducing the total thermal conductivity. Therefore, in this range even the Fourier's law is recovered as well, the Gaussian-type heat spreading density now becomes narrower and narrower. Such an understanding apparently provides more detailed evidence for relating the macroscopic heat transport properties and the underlying microscopic dynamics in the particular momentum-nonconserving ϕ^4 system.

In spite of above achievement, we should finally note that, to induce normal heat transport, generally one should rely on both the effects of nonlinearity and on-site potential, while all of the above understandings from DBs properties are just based on the quartic nonlinear on-site potential considered here. Although this is the mostly popular model used for demonstration the role of nonconserved momentum [35], we are still not sure that whether the proposed picture/explanation has its generality and can be extended to general models. Hence, in the next step we are attempted to study the case of on-site potential also including cubic anharmonicity. In addition, as to the relevant underlying picture, we here only provide strong evidences that, at zero temperature the mobile and immobile DBs can exist in the system, and their contributions to heat transport could be different. A further more complete picture about the phonon-DBs interaction at thermalized equilibrium state is still lacking. For this, a recent fractal Lévy heat transport picture as suggested in the nanoparticle embedded semiconductor alloys [12–15] would be insightful.

Acknowledgments

D.X. was supported by the National Natural Science Foundation of China (Grant No. 11575046); the Natural Science Foundation of Fujian Province, China (Grant No. 2017J06002); the Training Plan Fund for Distinguished Young Researchers from Department of Education, Fu-

jian Province, China, and the Qishan Scholar Research Fund of Fuzhou University, China. Stay of D.S. at IMSP RAS was partly supported by the Russian Science Foun-

dation, grant No. 14-13-00982. S.V.D. was supported by the grant of the Russian Science Foundation (No. 16-12-10175).

-
- [1] S. Lepri, R. Livi, and A. Politi, *Phys. Rep.* **377**, 1 (2003).
 - [2] A. Dhar, *Adv. Phys.* **57**, 457 (2008).
 - [3] S. Lepri, R. Livi, and A. Politi, *Thermal Transport in Low Dimensions*, Lecture Notes in Physics Vol. 921 (Springer, Berlin, 2016).
 - [4] Y. Hu, L. Zeng, A. J. Minnich, M. S. Dresselhaus, and G. Chen, *Nat. Nanotechnol.* **10**, 701 (2015).
 - [5] K. M. Hoogeboom-Pot, J. N. Hernandez-Charpak, E. H. Anderson, X. Gu, R. Yang, M. M. Murnane, H. C. Kapteyn, and D. Nard, *Proc. Natl. Acad. Sci.* **112**, 4846 (2015).
 - [6] C.-W. Chang, *Lecture Notes in Physics*, **921**, 305 (2016).
 - [7] V. Lee, C.-H. Wu, Z.-X. Lou, W.-L. Lee, and C.-W. Chang, *Phys. Rev. Lett.* **118**, 135901 (2017).
 - [8] T.-K. Hsiao, B.-W. Huang, H.-K. Chang, S.-C. Liou, M.-W. Chu, S.-C. Lee, and C.-W. Chang, *Phys. Rev. B* **91**, 035406 (2015).
 - [9] T.-K. Hsiao, H.-K. Chang, S.-C. Liou, M.-W. Chu, S.-C. Lee, and C.-W. Chang, *Nat. Nanotechnol.*, **8**, 534 (2013).
 - [10] J. Lee, J. Lim, and P. Yang, *Nano Lett.* **15**, 3273 (2015).
 - [11] Y.R. Koh, M. Shirazi-Hd, B. Vermeersch, A.M.S. Mohammed, J. Shao, G. Pernot, J.-H. Bahk, M.J. Manfra, and A. Shakouri, *Appl. Phys. Lett.* **109**, 243107 (2016).
 - [12] A.M.S. Mohammed, Y.R. Koh, B. Vermeersch, H. Lu, P. G. Burke, A. C. Gossard, and A. Shakouri, *Nano Lett.* **15**, 4269 (2015).
 - [13] M. Upadhyaya and Z. Aksamija, *Phys. Rev. B* **94**, 174303 (2016).
 - [14] B. Vermeersch, J. Carrete, N. Mingo, and A. Shakouri, *Phys. Rev. B* **91**, 085202 (2015).
 - [15] B. Vermeersch, A. M. S. Mohammed, G. Pernot, Y. R. Koh, and A. Shakouri, *Phys. Rev. B* **91**, 085203 (2015).
 - [16] C. de Tomas, A. Cantarero, A. F. Lopeandia, and F. X. Alvarez, *J. Appl. Phys.* **115**, 164314 (2014).
 - [17] C. de Tomas, A. Cantarero, A. F. Lopeandia, and F. X. Alvarez, *Proc. R. Soc. London A* **470**, 20140371 (2014).
 - [18] P. Torres, A. Torello, J. Bafaluy, J. Camacho, X. Cartoixa, and F. X. Alvarez, *Phys. Rev. B* **95**, 165407 (2017).
 - [19] Y. V. Kartashov, B. A. Malomed, and L. Torner, *Rev. Mod. Phys.* **83**, 247 (2011).
 - [20] S. Flach and C. R. Willis, *Phys. Rep.* **295**, 181 (1998).
 - [21] S. Flach and A. V. Gorbach, *Phys. Rep.* **467**, 1 (2008).
 - [22] S. V. Dmitriev, A. P. Chetverikov, and M. G. Velarde, *Phys. Status. Solidi B* **252**, 1682 (2015).
 - [23] S. V. Dmitriev, E. A. Korznikova, Yu. A. Baimova, and M. G. Velarde, *Phys. Usp.* **59**, 446 (2016).
 - [24] A. V. Savin, Y. S. Kivshar, and B. Hu, *Phys. Rev. B* **82**, 195422 (2010).
 - [25] A. V. Savin, B. Hu, and Y. S. Kivshar, *Phys. Rev. B* **80**, 195423 (2009).
 - [26] B. Liu, C. D. Reddy, J. Jiang, H. Zhu, J. A. Baimova, S. V. Dmitriev, and K. Zhou, *J. Phys. D: Appl. Phys.* **47**, 165301 (2014).
 - [27] B. Liu, F. Meng, C. D. Reddy, J. A. Baimova, N. Srikanth, S. V. Dmitriev, and K. Zhou, *RSC Advances* **5**, 29193 (2015).
 - [28] G. Casati, J. Ford, F. Vivaldi, and W. M. Visscher, *Phys. Rev. Lett.* **52**, 1861 (1984).
 - [29] T. Prosen and M. Robnik, *J. Phys. A* **25**, 3449 (1992).
 - [30] T. Hatano, *Phys. Rev. E* **59**, R1 (1999).
 - [31] S. Lepri, R. Livi, and A. Politi, *Phys. Rev. Lett.* **78**, 1896 (1997).
 - [32] B. Li, G. Casati, J. Wang, and T. Prosen, *Phys. Rev. Lett.* **92**, 254301 (2004).
 - [33] T. Prosen and D. K. Campbell, *Chaos* **15**, 015117 (2005).
 - [34] T. Prosen and D. K. Campbell, *Phys. Rev. Lett.* **84**, 2857 (2000).
 - [35] B. Hu, B. Li, and H. Zhao, *Phys. Rev. E* **57**, 2992 (1998).
 - [36] B. Hu, B. Li, and H. Zhao, *Phys. Rev. E* **61**, 3828 (2000).
 - [37] O. Narayan and S. Ramaswamy, *Phys. Rev. Lett.* **89**, 200601 (2002).
 - [38] Y. Zhong, Y. Zhang, J. Wang, and H. Zhao, *Phys. Rev. E* **85**, 060102(R) (2012).
 - [39] S. Chen, Y. Zhang, J. Wang, and H. Zhao, *J. Stat. Mech.* (2016) 033205.
 - [40] A. V. Savin and Y. A. Kosevich, *Phys. Rev. E* **89**, 032102 (2014).
 - [41] S. G. Das, A. Dhar, and O. Narayan, *J. Stat. Phys.* **154**, 204 (2014).
 - [42] L. Wang, B. Hu, and B. Li, *Phys. Rev. E* **88**, 052112 (2013).
 - [43] Z. Rieder, J. L. Lebowitz, and E. Lieb, *J. Math. Phys.* **8**, 1073 (1967).
 - [44] A. M. Krivtsov, *Doklady Physics*, **60**, 407 (2015).
 - [45] V. A. Kuzkin and A. M. Krivtsov, *Doklady Physics*, **62**, 85 (2017).
 - [46] V. A. Kuzkin and A. M. Krivtsov, *Phys. Solid State* **59**, 1051 (2017).
 - [47] S. Chen, J. Wang, G. Casati, and G. Benenti, *Phys. Rev. E* **90**, 032134 (2014).
 - [48] D. SK. Sato, *Phys. Rev. E* **94**, 012115 (2016).
 - [49] J. Jiang and H. Zhao, *J. Stat. Mech.* (2016) 093208.
 - [50] L. H. Liang and B. Li, *Phys. Rev. B* **73**, 153303 (2006).
 - [51] C. Giardinà, R. Livi, A. Politi, and M. Vassalli, *Phys. Rev. Lett.* **84**, 2144 (2000).
 - [52] O. V. Gendelman and A. V. Savin, *Phys. Rev. Lett.* **84**, 2381 (2000).
 - [53] S. G. Das and A. Dhar, *arXiv:1411.5247v2* (2015).
 - [54] H. Spohn, *arXiv:1411.3907v1* (2014).
 - [55] D. Roy, *Phys. Rev. E* **86**, 041102 (2012).
 - [56] G. R. Lee-Dadswell, E. Turner, J. Ettinger, and M. Moy, *Phys. Rev. E* **82**, 061118 (2010).
 - [57] C. Giardinà and J. Kurchan, *J. Stat. Mech.: Theory Exp.* (2005) P05009.
 - [58] D. Xiong, *Europhys. Lett.* **113**, 140002 (2016).
 - [59] D. Xiong, *J. Stat. Mech.: Exp. Theor.* (2016) 043208.
 - [60] G. P. Tsironis, A. R. Bishop, A. V. Savin, and A. V. Zolotaryuk, *Phys. Rev. E* **60**, 6610 (1999).
 - [61] G. P. Tsironis and S. Aubry, *Phys. Rev. Lett.* **77**, 5225 (1996).

- [62] H. Zhao, Phys. Rev. Lett. **96**, 140602 (2006).
- [63] V. Zaburdaev, S. Denisov, and J. Klafter, Rev. Mod. Phys. **87**, 483 (2015).
- [64] V. Zaburdaev, S. Denisov, and P. Hänggi, Phys. Rev. Lett. **106**, 180601 (2011).
- [65] D. Forster, *Hydrodynamic Fluctuations, Broken Symmetry, and Correlation Functions* (Benjamin, New York, 1975).
- [66] J. P. Hansen and I. R. McDonald, *Theory of Simple Liquids*, 3rd ed. (Academic, London, 2006).
- [67] S. Chen, Y. Zhang, J. Wang, and H. Zhao, Phys. Rev. E **87**, 032153 (2013).
- [68] D. Xiong, Phys. Rev. E **95**, 042127 (2017).
- [69] S. G. Das, A. Dhar, K. Saito, C. B. Mendl, and H. Spohn, Phys. Rev. E **90**, 012124 (2014).
- [70] H. Spohn, J. Stat. Phys. **154**, 1191 (2014).
- [71] D. Xiong and E. Barkai, arXiv:1606.04602v2 (2016). The updated version is ‘D. Xiong, F. Thiel, and E. Barkai, Phys. Rev. E **96**, 022114 (2017)’, while the concept of “phonon random walks” there has now not been emphasized implicitly.
- [72] A. J. Sievers and S. Takeno, Phys. Rev. Lett. **61**, 970 (1988).
- [73] A. A. Kistanov, R. T. Murzaev, S. V. Dmitriev, V. I. Dubinko, and V. V. Khizhnyakov, JETP Lett. **99**, 353 (2014).
- [74] S. A. Arrhenius, Z. Phys. Chem. **4**, 96 (1889).
- [75] Y. Li, S. Liu, N. Li, P. Hänggi, and B. Li, New J. Phys. **17**, 043064 (2015).
- [76] Shi-xiao W. Jiang, H. H. Lu, D. Zhou, and D. Cai, New J. Phys. **18**, 083028 (2016).
- [77] D. Xiong, J. Wang, Y. Zhang, and H. Zhao, Phys. Rev. E **85**, 020102 (2012); D. Xiong, Y. Zhang, and H. Zhao, *ibid* **88**, 052128 (2013); *ibid* **90**, 022117 (2014).